http://dx.doi.org/10.1016/j.jmatprotec.2019.05.012

Characterization of the microscale forming limit for metal foils considering free surface roughening and failure mechanism transformation

C. Cheng[1], M. Wan[1], B. Meng[1,*], M.W. Fu[2,#]

[1] School of Mechanical Engineering and Automation, Beihang University, Beijing 100191, P.R. China

[2] Department of Mechanical Engineering, The Hong Kong Polytechnic University, Hung Hom, Kowloon, Hong Kong, P.R. China

[*]Corresponding author. Tel.: +86-10-82338613. E-mail address: mengbao@buaa.edu.cn

[#]Corresponding author. Tel.: 852-27665527. E-mail address: mmmwfu@polyu.edu.hk

Abstract

The ductile fracture behavior of metal foils is greatly affected by size effect and free surface roughening phenomenon. To explore and characterize the effects induced by the two factors on the formability and failure mechanism in microscale plastic deformation, the micro-scaled forming limit of metal foils (μ-FLC) was investigated by physical experiment and theoretical modeling. A sectionalized failure criterion was first developed based on the original Considère and M-K models via considering the coupled effect of free surface roughening and failure mechanism transformation at microscale. In detail, the modified Considère criterion coupled with the free surface roughening was proposed to predict the right-hand-side μ-FLC, while the modified PMC model by adjusting the surface roughness parameter was developed to construct the left-hand-side μ-FLC. The physical experiment suggests that the magnitude of surface roughness caused by free roughening can be up to 10~20% of foil thickness until the fracture of the sample. In addition, the surface roughness is proportional to the effective strain and grain size, while the material constant is independent of grain size and foil thickness. The failure mechanism of metal foils in microscale deformation tends to be transformed from localized necking to diffuse instability with the change of stress state from uniaxial tension to equi-biaxial tension. Furthermore, the increase of grain size or the decrease of foil thickness promotes the transformation of failure pattern from the localized necking to diffuse instability. The experimentally determined μ-FLCs shift down with the increasing grain size and the decreasing foil thickness and a much scattered limit strain is observed with one grain or less grainover the thickness direction of metal foils. The original Considère criterion and M-K model are not suitable for prediction of μ-FLC as

they do not consider the significant effect of free surface roughening and failure mode transformation on the microformability of metal foils. The developed criterion was validated and corroborated by the comparison between the theoretically determined μ-FLCs and the experimental ones. All of these findings advance the insight into the ductile fracture and formability of metal foils affected by size effect and free surface roughening phenomenon and help to improve the microformed product quality and facilitate the applications of microforming technologies.

Keywords: Micro-scaled forming limit; Size effect; Free surface roughening; Failure mechanism; Failure criterion.

1. Introduction

With the rapid development of production miniaturization in various industrial fields, the meso/micro-scaled workpieces with at least two dimensions less than 1 mm are ubiquitously used in various microsystems (Razali and Qin, 2013). To fabricate these microparts, a variety of micromanufacturing methods including micromachining, micro additive processes and LIGA have been developed (Jain et al., 2014). Considering the distinct advantages such as excellent mechanical property, low cost, high productivity and minimized or zero material loss, microforming process has become one of the most promising manufacturing technologies (Vollertsen et al., 2006). However, the material properties and quality of the microformed parts are profoundly influenced by the so-called size effect when the workpiece dimension is scaled down from macro to micro level. Currently, the size effect on plastic deformation behavior has been extensively studied and many constitutive models have been proposed to describe the microscale deformation behavior in microforming (Meng and Fu, 2015; Peng et al., 2017a). The size effect on fracture behavior of ultrathin metal foils, however, has not yet been explored thoroughly. Since the fracture behavior is related to manufacturability and micro-formed part quality and properties, it is thus necessary to further explore the micro/meso-scaled forming limit in microforming process of metal foils.

The conception of forming limit curve (FLC) is widely used to assess the sheet metal formability in macro-scale domain and employed to describe the forming performance of metal foils. It is defined as the microscale FLC (μ-FLC). According to prior arts, there are two methods to obtain the μ-FLC including experimental determination and theoretical calculation. In the experimental determination, Xu et al. (2015b; 2014) constructed the experimental μ-FLC of copper sheets with the thicknesses of 0.1, 0.2 and 0.4 mm by using the miniaturization of Holmberg and Marciniak methods. Gau et al. (2013) carried out a series of microscale limit dome height (LDH) tests using the stainless steel 304 foils with the thickness of 50 μm to obtain the experimental FLCs. According to the investigation of Bong et al. (2012), the FLC of ferritic stainless steel sheet with the thickness of 0.1 mm was determined by the modified Marciniak test and the conventional ASTM standard test. Sène et al. (2013) designed a micro-drawing press based on the Marciniak principle to acquire the experimental FLCs of pure aluminum and its alloy with the thickness of 0.2 mm.

Since the experimental determination of FLC is complex, time-consuming and expensive, it is gradually replaced by the theoretical calculation of FLC. At present, several conventional fracture criteria had been developed to predict the failure behavior of metal foils and further

to construct the FLCs. Peng et al. (2017b) employed a number of the most widely-used failure criteria including instability models, ductile facture criteria and the Gurson-Tvergaard-Needleman (GTN) model to evaluate their applicability under the microscale deformation condition. By considering the geometrical and microstructural effects on the void evolution, Xu et al. (2015b) developed an extended GTN-Thomason model to predict FLCs of copper sheets with the thicknesses of 0.1, 0.2 and 0.4 mm. They suggested that the damage-coupled model is no longer applicable for the scenario with grain number in thickness direction less than two because the microvoids evolution is not to be the major failure mechanism in that case. In addition, Ran and Fu (2014) established a hybrid model for prediction of the ductile fracture of multiphase alloys in micro-scaled plastic deformation. Based on the experimental FLCs and the conventional ductile fracture criterion, Chen et al. (2010) proposed two new models to predict the forming limit of stainless steel 304 foils. Abe (2014) assumed that the geometric imperfection adopted in M-K model is caused by the difference in *r*-value for the respective regions of thin metal sheets, and suggested that the theoretical FLC can be calculated by the modified M-K model. Furthermore, Meng et al. (2015) used five uncoupled fracture criteria to predict the micro-scaled shearing and blanking processes. However, the theoretical μ-FLCs based on the conventional fracture criteria usually are not consistent with the experimental results, which is attributed to the fact that the failure mechanism at micro/meso scale is different from that in macroscale. Especially, the effect of free surface roughness on the forming limit of thin sheet metals should not be ignored in micro/meso-scale forming.

Unlike the thick sheet metals, the effect of surface roughness of metal foils in plastic deformation is significant (Furushima et al., 2018; Furushima et al., 2014; Manabe et al., 2008). It is found that the free surface roughness is increased with the plastic deformation since the surface grains are less restricted in deformation and able to deform with more degrees of freedom (Furushima et al., 2011; Guangnan et al., 1990; Osakada and Oyane, 1971). Therefore, the interaction of free surface roughening and size effect should be considered in prediction of microscale forming limit. In tandem with this, Parmar et al. (1977) proposed a PMC model by incorporating the surface roughness evolution into the M-K model. In this model, the free surface roughness is characterized by pyramidal ridges. Moreover, Yamaguchi et al. (1995) studied the effect of interstage polishing of surface roughness on the forming limit of metal foils and found that the forming limit was improved by polishing the surface roughness before the onset of localized necking. According to the investigation done

by Stachowicz (2016), the material inhomogeneity caused by surface roughness and internal defects was used to calculate the theoretical forming limit strains based on the M-K theory. It is found that the effect of surface roughness on the level of μ-FLC is more prominent than that caused by void growth. In addition, Nurcheshmeh and Green (2016) established the relationship between the initial imperfection factor in the M-K model and the surface roughness to predict the FLC. Al-Qureshi et al. (2005) employed the modified Al-Qureshi/Bressan theoretical model to study the influence of surface roughness on the onset of plastic instability and necking conditions considering the effect of surface asperities. By comparing with the experimental forming limit, Jain et al. (1996) found that the PMC model combined Voce hardening law and surface roughness parameter can accurately predict the FLC. Therefore, the failure models coupled with the free surface roughening evolution can accurately describe the fracture behavior of metal foils. However, the relation between the surface roughness and failure mechanism under different stress states has not yet been sufficiently revealed and clarified. The determination of surface roughness parameter is also ambiguous, which is the first issue to be addressed in exploring how surface roughening and failure mechanism affect FLCs.

Based on the above review of the previous researches, the free surface roughening phenomenon is aggravated with the miniaturization of deformation process, which in turn affects the ductile fracture behavior and the transformation of failure mechanism. In addition, there is still lack of failure model for accurate prediction of the μ-FLCs of metal foils when the ratio of foil thickness to grain size is two or less than two. The research was thus conducted is to explore the effect of surface roughness on the forming limit of metal foils and the transformation of failure mechanism under different stress states, and further establish the failure criterion for accurately predicting of μ-FLC of metal foils, especially for the foils with less than one grain across the thickness. To this end, the micro forming limit experiments were first carried out and the experimental μ-FLCs of the stainless steel 304 foils with different thicknesses and grain sizes were constructed. The relationship between failure mechanism and stress state was discussed. The original and modified failure criteria considering the free surface roughening phenomenon were adopted to calculate the theoretical μ-FLC. By comparing the experimental and theoretical μ-FLC, the effect of surface roughening on forming limit is extensively analyzed. Finally, the evolution of the critical stress state for distinguishing diverse failure patterns with different material conditions was also analyzed. Research methodology and experimental procedures

2.1 Research methodology

Fig. 1 presents the research framework adopted in this research. The stress-strain behavior and the relationship between surface roughness and plastic strain of metal foils were first established based on the uniaxial tensile test. The micro forming limit experiment was then conducted to analyze the failure mechanism of metal foils and further to construct the experimental FLCs. The theoretical μ-FLCs based on the conventional failure criteria were compared with the experimental ones to verify their validity at microscale. According to the error mechanism of the traditional failure modes and the transformation of failure pattern at diverse stress states, the microscale forming limit of metal foils was predicted by the modified Considère and PMC models coupling with free surface roughening and size effect. In addition, the critical stress state for distinguishing the diverse failure mechanisms was proposed to sectionally predict the μ-FLCs based on the transformation of failure mechanism.

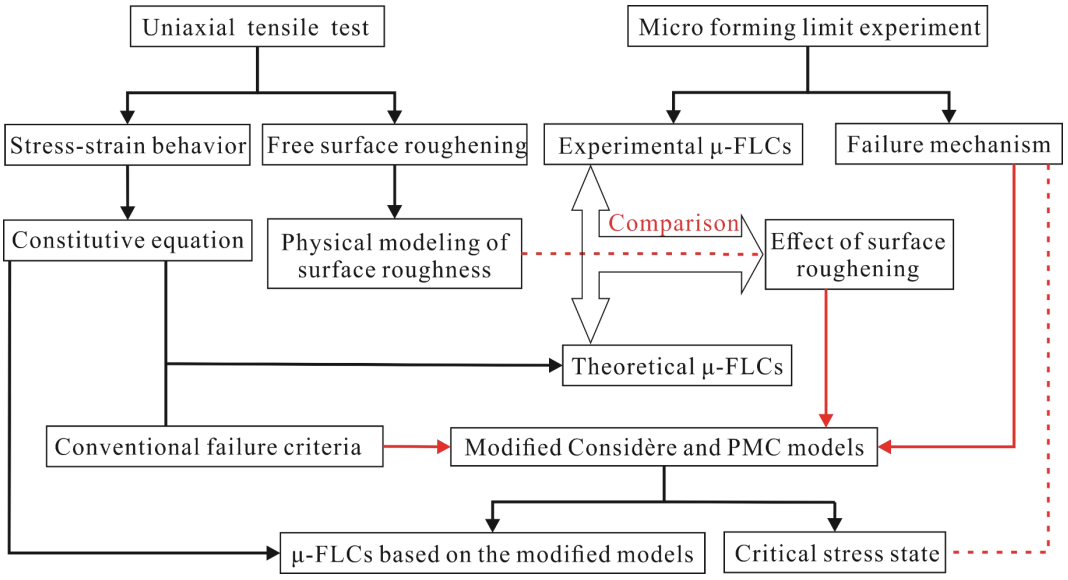

Fig. 1 Flow chart of the research methodology.

In the research, the austenitic stainless steel 304 foils were used to investigate the forming limit of metal foils, and its chemical composition is given in **Table 1**. The as-received materials with the thicknesses of 200, 120 and 50 μm were annealed in vacuum environment at different temperatures to produce various grain sizes. The heated-treated samples were then etched with the solution of 10% oxalic acid to reveal the austenite grain boundaries. The detailed annealing conditions and the corresponding grain sizes are listed in **Table 2**. The cross-section microstructures of the stainless steel 304 foils are presented in **Fig. 2**.

Table 1 Chemical compositions of the austenitic stainless steel 304 foils.

Nominal composition (wt. %)						
C	Si	Mn	P	S	Cr	Ni
0.049	0.525	1.083	0.033	0.003	18.180	8.011

Table 2 Annealing parameters and the fitting parameters of Voce equation.

t_0 (μm)	Annealing parameters		Grain size d_0 (μm)	σ_y (MPa)	a	b	c
200	(I)	1000 °C for 1 h	48.98	1401	0.823	-2.01	0.488
	(II)	1050 °C for 1 h	64.83	1045	0.781	-2.85	0.480
	(III)	1100 °C for 1.5 h	94.87	877.7	0.768	-3.41	0.500
120	(IV)	1000 °C for 1 h	42.57	953.8	0.762	-3.50	0.524
	(V)	1050 °C for 1 h	60.27	873.7	0.763	-3.55	0.496
	(VI)	1100 °C for 1.5 h	68.41	648.1	0.731	-5.19	0.516
50	(VII)	1000 °C for 1 h	34.90	912.0	0.765	-3.48	0.519
	(VIII)	1050 °C for 1 h	52.63	682.8	0.764	-4.21	0.498

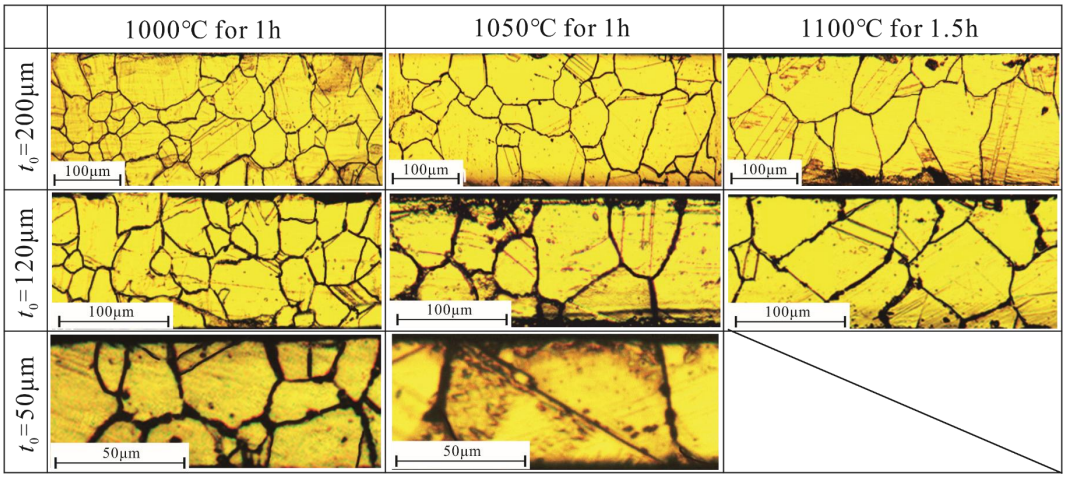

Fig. 2. Microstructures of stainless steel 304 foils.

2.2 Uniaxial tensile test

To obtain the flow behavior of the austenitic stainless steel 304 foils, uniaxial tensile tests were conducted on a tensile testing machine. The shape and geometric dimension of the specimens were designed based on the ASTM E8 standard andare shown in **Fig. 3**. The specimens were cut along three different directions, i.e., 0°, 45° and 90° to rolling direction. During the tensile test, the digital image correlation (DIC) system was employed to measure the deformation fields at the surface of metal foil. The tensile tests were conducted at a constant strain rate of 0.083 s^{-1}. **Fig. 4** shows the stress-strain curves along the rolling

direction under diverse material conditions. The obvious reduction of flow stress with increasing grain size and decreasing foil thickness can be found, which can be explained by the so-called surface layer model (Lai et al., 2008; Xu et al., 2015a). In addition, the mechanical properties of metal foils along different directions are also summarized in **Table 3**. It is concluded that the annealed stainless steel 304 foils are not mechanically isotropic especially with the larger grain size and the thinner foil thickness conditions. The Voce law equation designated in Eq.(1) was then used to fit the uniaxial stress-strain curves and can describe the saturation behavior of working hardening in the large strain condition.

$$\sigma=\sigma_y(1-a\exp(b\varepsilon)) \tag{1}$$

where σ_y, a and b are the fitting parameters and summarized in **Table 2**. The corresponding fitting curves and the comparisons with the experimental results are shown in **Fig. 4**.

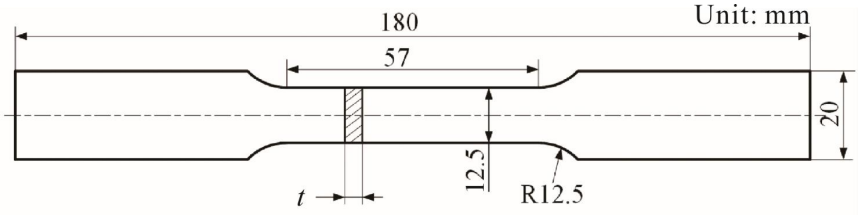

Fig. 3 The shape and geometric dimensions of the specimens.

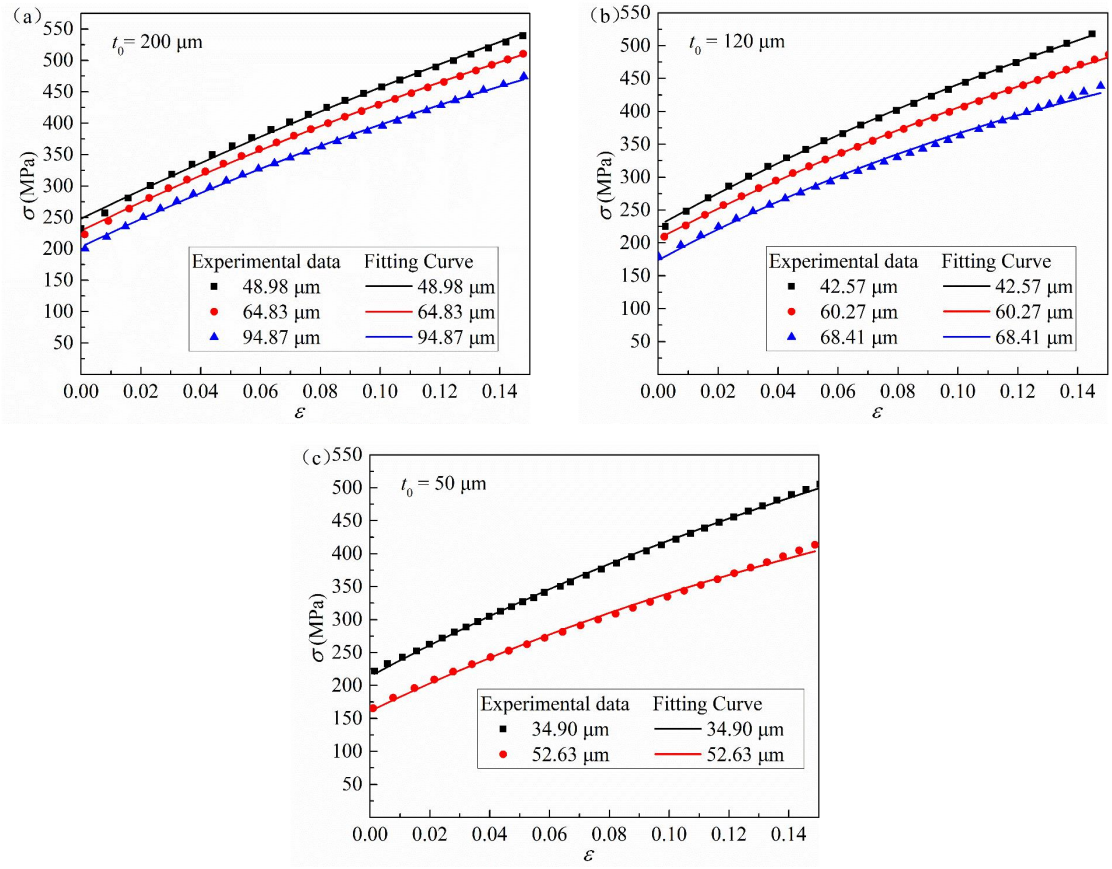

Fig. 4 The experimental and the fitted stress-strain curves using the tensile specimens with different foil thicknesses: (a) 200 μm; (b) 120 μm and (c) 50 μm.

Table 3 Mechanical properties of the austenitic stainless steel 304 foils.

Material conditions	σ_0 (MPa)	σ_{45} (MPa)	σ_{90} (MPa)	r_0	r_{45}	r_{90}
(I)	240.1	238.0	233.2	0.952	0.981	0.962
(II)	224.5	215.3	220.0	0.944	0.971	0.948
(III)	202.0	189.8	188.7	0.902	0.952	0.897
(IV)	245.3	240.2	244.2	0.930	0.904	0.920
(V)	873.7	209.4	206.3	0.919	0.938	0.943
(VI)	648.1	173.2	170.4	0.899	0.918	0.882
(VII)	912.0	254.1	250.4	0.916	0.996	0.941
(VIII)	682.8	169.6	161.3	0.948	0.894	0.878

2.3 Surface roughness measurement

According to the previous studies (Fukui and Nakanishi, 2008; Pham et al., 2015), the evolution of free surface roughening with plastic deformation is independent of stress state. Considering the fact that uniaxial tensile test can be carried out easily, the surface roughness under the uniaxial stress state was analyzed at diverse strain levels. In measuring of the surface roughness, the uniaxial tensile test was suspended at a pre-determined strain and the sample was then taken out from the uniaxial testing machine. The surface roughness of the deformed sample was then measured by the contact surface roughness meter (TR200S). The pre-determined strain was set with an interval of 10% from the initial state to fracture. Finally, the evolution of surface roughness with plastic deformation was evaluated. **Fig. 5** presents the relationship between the surface roughness R_z (maximum peak-to-valley height) and the true strain of the metal foils under diverse material conditions. It is found that the surface roughness is increased linearly with true strain. Prior studies (Furushima et al., 2014; Mahmudi and Mehdizadeh, 1998) have demonstrated that the surface roughness R_z induced by the free surface roughening is proportional to the effective strain ε_{eq} and the initial grain size d_0, designated as:

$$R_z = c d_0 \varepsilon_{eq} + R_0 \tag{2}$$

where c is a material constant depending on the slip characteristic of materials and R_0 is the initial surface roughness. The constant c was calculated and is shown in **Table 2** under diverse material conditions. It is observed that the value of c in the range of $c = 0.5 \pm 0.02$ is independent of grain size and foil thickness, which is consistent with the finding of Mahmudi and Mehdizadeh (1998). On the other hand, it is shown that the magnitude of surface

roughness can reach 10~20% of foil thickness until the fracture of specimens, which has a strong effect on the plastic instability and ductile fracture of metal foils.

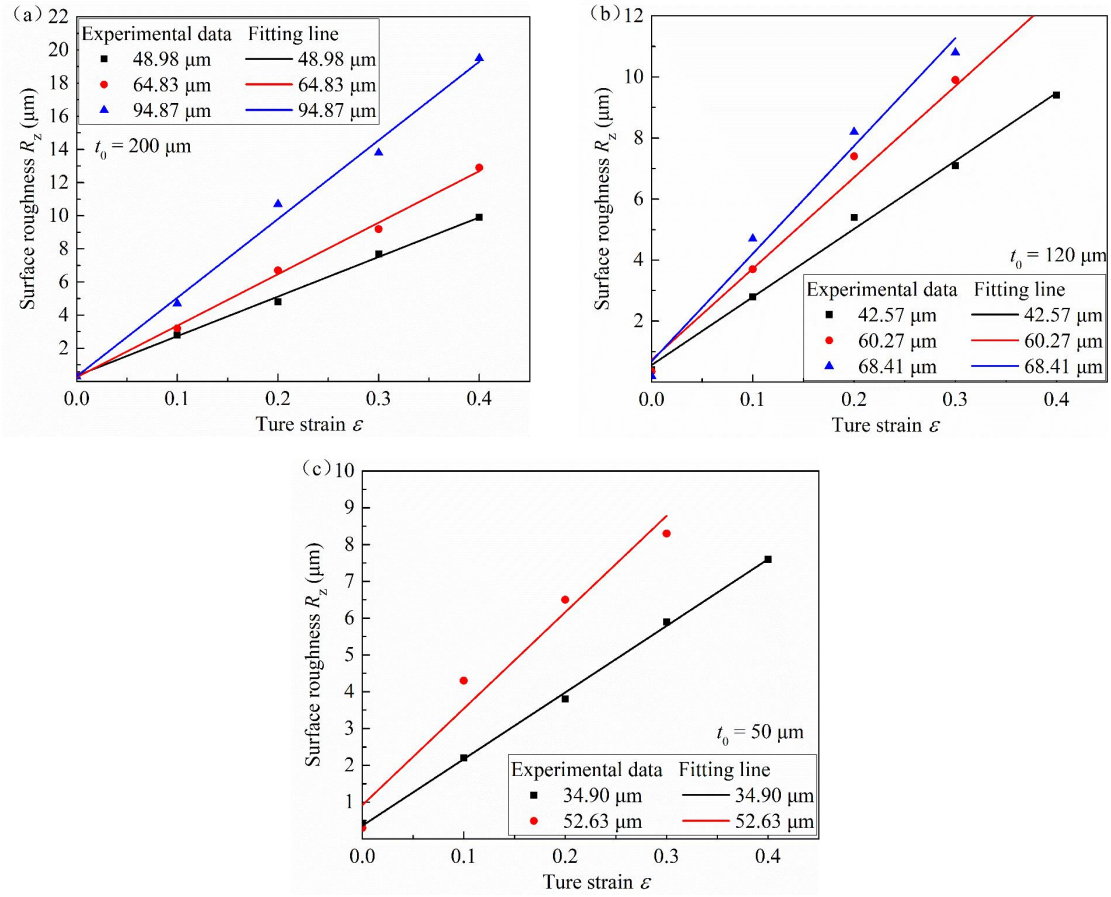

Fig. 5 Relationship between the surface roughness R_z and true strain for metal foils with different thicknesses: (a) 200 μm; (b) 120 μm and (c) 50 μm.

2.4 Micro forming limit experiment

To study the forming limit of metal foils, Holmberg method and the modified Marciniak test were employed to obtain the left-hand-side FLD and the right-hand-side FLD, respectively. For the two experimental methods, the problems such as wrinkle, buckle, friction and positioning error, which are usually observed in the Nakazima test of metal foils, can be avoided. The experimental setup and the dimensions of specimens are illustrated in **Fig. 6**. For the Holmberg method, the forming limit tests can be conducted on the uniaxial tensile testing machine. In the modified Marciniak test, the specimens were deformed indirectly through a washer with a hole at the center. Since the metal foil is in the micro/meso scale, the dimensions of the tools were scaled down, as depicted in **Fig. 6**. The limit strain was measured by the DIC method (2017b; 2015b).

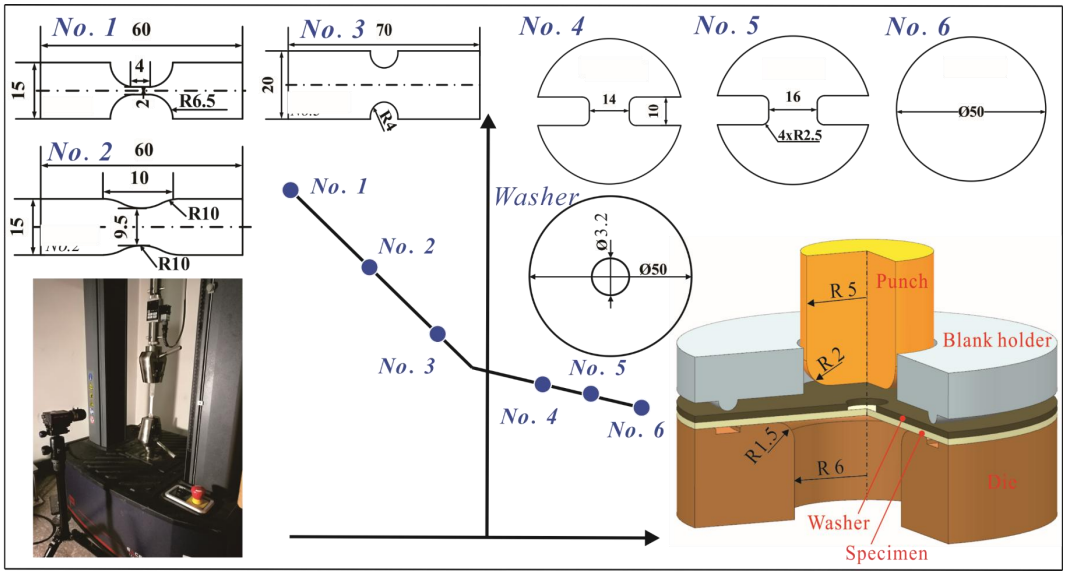

Fig. 6 Experimental setup and the dimensions of specimens.

2. Theoretical models for prediction of μ-FLC

3.1 Physical modeling of surface roughening

In microforming process, free surface roughening has a significant effect on the ductile fracture behavior of metal foils. To reasonably and accurately predict the forming limit of metal foils, it is necessary to establish a physical model for characterizing free surface roughness. **Fig. 7**(a) illustrates the 3D surface profile of the uniaxial tensile specimens measured by a confocal laser microscope. Based on the practical surface profile, the pyramidal shape was employed to construct the surface roughness, as indicated in **Fig. 7**(b). The stretched rectangular element of metal foils has the length l_1 and the width l_2 and is subjected to the tensile load F_1 and F_2 ($F_1 \geq F_2$). The base of a pyramid volume has the width m and the height of R_z. According to the assumption from Parmar (1977), the part of the surface roughening cannot bear the tensile load. With the development of plastic deformation, the surface roughness R_z is increased and the shape of pyramid remains. Thus, the actual load-bearing matrix is lower than the volume of metal foil, especially under the large plastic strain condition.

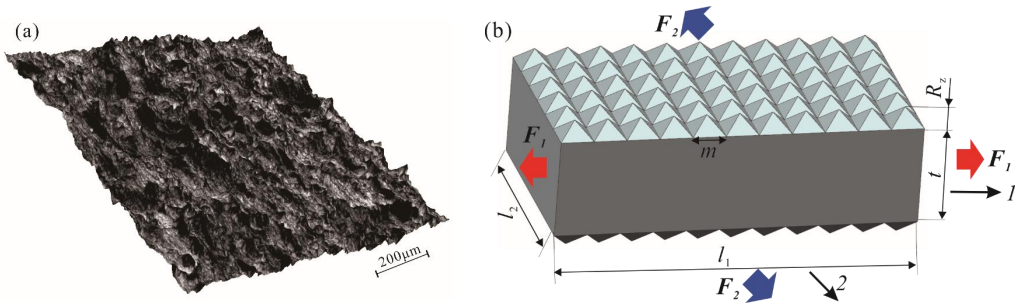

Fig. 7 3D surface profile of free surface roughening: (a) Experimental topography and (b) Geometry modeling.

In addition, the initial surface roughness can be ignored before the plastic deformation. The overall volume of metal foil is $t_0 l_{1\text{-}0} l_{2\text{-}0}$ and t_0 is the initial thickness of metal foil. As the plastic deformation proceeds, the overall volume Vol with the plastic strain of ε_{eq} can be denoted as:

$$Vol = t l_1 l_2 + 2 * \frac{1}{3} m R_z l_2 * (l_1 / m) \tag{3}$$

where l_1 and l_2 are the strained lengths along the *1* and *2* axes respectively with the plastic strain ε_{eq}. R_z is the surface roughness. t is the minimum thickness of metal foil excluding the surface roughness. Considering the principle of volume of constancy, Eq. (3) is reduced as:

$$\frac{t}{t_0} = \frac{l_{1-0} l_{2-0}}{l_1 l_2} - \frac{2}{3} \frac{R_z}{t_0} \tag{4}$$

Substituting Eq. (2) into Eq. (4), the following equation is obtained.

$$\frac{t}{t_0} = \exp(-\varepsilon_1 - \varepsilon_2) - \frac{2}{3}\left(c \frac{d_0}{t_0} \varepsilon_{eq} + \frac{R_0}{t_0}\right) \tag{5}$$

where ε_1 and ε_2 are the major and minor strains, respectively. Considering the anisotropic properties of yield stress and the *r*-value of the austenitic stainless steel 304 foils, the Yld2000-2d yield criterion (Barlat et al., 2003) was employed to characterize the yield behaviors, which is formulated as:

$$\phi = \phi' + \phi'' = 2\sigma_e^m \tag{6}$$

where

$$\phi' = |Y_1' - Y_2'|^m, \quad \phi'' = |2Y_2'' + Y_1''|^m + |2Y_1'' + Y_2''|^m \tag{7}$$

Y_i' and Y_j'' $(i, j = 1, 2)$ are the principal values of the matrices X' and X'':

$$\begin{cases} Y_i' = \dfrac{1}{2}(X_{11}' + X_{22}' \pm \sqrt{(X_{11}' - X_{22}')^2 + 4X_{12}'^2}) \\ Y_i'' = \dfrac{1}{2}(X_{11}'' + X_{22}'' \pm \sqrt{(X_{11}'' - X_{22}'')^2 + 4X_{12}''^2}) \end{cases} \tag{8}$$

The elements of X' and X'' were obtained by using the linear transformation of stress components, as shown in Eq. (9)

$$\begin{cases} X' = L'\sigma \\ X'' = L''\sigma \end{cases} \tag{9}$$

where

$$\begin{bmatrix} L_{11}' \\ L_{12}' \\ L_{21}' \\ L_{22}' \\ L_{66}' \end{bmatrix} = \begin{bmatrix} 2/3 & 0 & 0 \\ -1/3 & 0 & 0 \\ 0 & -1/3 & 0 \\ 0 & 2/3 & 0 \\ 0 & 0 & 1 \end{bmatrix} \begin{bmatrix} \alpha_1 \\ \alpha_2 \\ \alpha_7 \end{bmatrix}$$

$$\begin{bmatrix} L_{11}'' \\ L_{12}'' \\ L_{21}'' \\ L_{22}'' \\ L_{66}'' \end{bmatrix} = \frac{1}{9} \begin{bmatrix} -2 & 2 & 8 & -2 & 0 \\ 1 & -4 & -4 & 4 & 0 \\ 4 & -4 & -4 & 1 & 0 \\ -2 & 8 & 2 & -2 & 0 \\ 0 & 0 & 0 & 0 & 9 \end{bmatrix} \begin{bmatrix} \alpha_3 \\ \alpha_4 \\ \alpha_5 \\ \alpha_6 \\ \alpha_8 \end{bmatrix} \tag{10}$$

where m is the non-quadratic exponent of materials and α_1 - α_8 are the independent anisotropy parameters. In this research, m is set to 8 foraustenitic stainless steel 304 foil. The eight anisotropy parameters, α_1 - α_8, can be solved based on the eight material characteristic parameters from the uniaxial tensile tests along the rolling, diagonal and transversal directions, together with the equi-biaxial tensile test (σ_0, σ_{45}, σ_{90}, σ_b, r_0, r_{45}, r_{90}, r_b). **Table 4** presents the calculated anisotropy parameters of Yld2000-2d for the metal foils.

Based on the associated flow rule, the relationship among the plastic strain increments is described as:

$$\frac{d\varepsilon_1}{\varphi_1} = \frac{d\varepsilon_2}{\varphi_2} = \frac{d\varepsilon_3}{\varphi_3} = \frac{d\varepsilon_{eq}}{\varphi} \tag{11}$$

where $\varphi_1 = \dfrac{\partial \phi}{\partial \sigma_{11}}$, $\varphi_2 = \dfrac{\partial \phi}{\partial \sigma_{22}}$, $\varphi_3 = -(\varphi_1 + \varphi_2)$ and $\varphi = \dfrac{\partial \phi}{\partial \sigma_e}$.

Table 4 Yld2000-2d yield criterion anisotropy parameters.

t_0 (μm)	d_0 (μm)	α_1	α_2	α_3	α_4	α_5	α_6	α_7	α_8
200	48.98	0.9686	1.0569	0.9779	1.0188	1.0207	1.0774	1.0086	0.9922
	64.83	0.9832	1.0378	1.0228	1.0220	1.0281	1.1167	1.0414	1.0543
	94.87	0.9232	1.1400	1.0083	1.0565	1.0461	1.1716	1.0602	1.0704
120	42.57	1.0020	1.0053	1.0807	1.0238	1.0285	1.1238	1.0193	0.9994
	60.27	0.9643	1.0699	1.0324	1.0333	1.0372	1.1475	1.0156	0.9737
	68.41	0.9391	1.1303	1.1204	1.0747	1.0694	1.2865	1.0234	0.9007
50	34.90	1.0275	0.9367	0.9999	0.9841	0.9988	0.9871	1.0121	1.0471
	52.63	0.9935	1.0539	1.1458	1.0598	1.0584	1.2789	1.0541	0.9859

In terms of the associated flow rule, i.e., Eq. (11) and the total strain theory of plasticity, the change rate of of the minimum thickness t is obtained by differentiating Eq. (5).

$$\frac{dt}{t}=\frac{(-\frac{\varphi_1}{\varphi}-\frac{\varphi_2}{\varphi})\exp(-\frac{\varphi_1}{\varphi}\varepsilon_{eq}-\frac{\varphi_2}{\varphi}\varepsilon_{eq})-\frac{2}{3}c\frac{d_0}{t_0}}{\exp(-\frac{\varphi_1}{\varphi}\varepsilon_{eq}-\frac{\varphi_2}{\varphi}\varepsilon_{eq})-\frac{2}{3}(c\frac{d_0}{t_0}\varepsilon_{eq}+\frac{R_0}{t_0})}d\varepsilon_{eq} \tag{12}$$

In Eq. (12), (dt/t) is not a plastic strain increment in the thickness direction. Ignoring the effect of surface roughness in the overall volume of metal foils, Eq. (5) is further expressed as:

$$\varepsilon_3=-\varepsilon_1-\varepsilon_2 \tag{13}$$

which satisfies the assumption of volume constancy of the macroscale deformation of sheet metal with thick thickness. (Eqs.(5) and (13) are quite different in terms of format. Pls pay attention to this!

3.2 Considère criterion

For Considère criterion, necking is assumed to happen until the load acting on a certain foil cross section and reaching its maximum value. But the metal foils will not be able to support the higher load along this cross section (Zhang and Wang, 2012). The necking is perpendicular to the major strain direction according to Tadros and Mellor (1975). The force equilibrium equation before the formation of necking is designated as:

$$F_1=\sigma_1 A_1=\sigma_1 l_2 t \tag{14}$$

where σ_1 is the principal stress along the axis-*1*. When the load is the maximum ($dF_1 = 0$), the diffuse instability condition is formulated as:

$$\frac{d\sigma_1}{\sigma_1}=-(d\varepsilon_2+\frac{dt}{t}) \tag{15}$$

When the plastic deformation is up to load instability, the stress state remains constant,

which implies that σ_1 is proportional to σ_e and the following relationship is established:

$$\frac{d\sigma_2}{d\sigma_1}=\frac{\sigma_2}{\sigma_1}=\alpha \tag{16}$$

where α is the stress state that remains constant during the deformation.

In the homogeneous deformation stage, the increase of equivalent stress, $d\sigma_e$, can be expressed by the principal stress increments $d\sigma_1$ and $d\sigma_2$.

$$d\sigma_e=\beta_1 d\sigma_1+\beta_2 d\sigma_2 \tag{17}$$

where $\beta_1=\frac{\partial\sigma_e}{\partial\sigma_1}=\frac{\varphi_1}{\varphi}$, $\beta_2=\frac{\partial\sigma_e}{\partial\sigma_2}=\frac{\varphi_2}{\varphi}$.

By differentiating Eq. (1), the increase of equivalent stress can also be expressed as:

$$\frac{d\sigma_e}{\sigma_e}=\frac{-ba\exp(b\varepsilon_{eq})}{1-a\exp(b\varepsilon_{eq})}d\varepsilon_{eq} \tag{18}$$

Combining Eqs. (15), (16), (17) and (18), the following equation is obtained:

$$\varphi_e\frac{-ba\exp(b\varepsilon_{eq})}{1-a\exp(b\varepsilon_{eq})}d\varepsilon_{eq}=(\beta_1+\alpha\beta_2)(-d\varepsilon_2-\frac{dt}{t}) \tag{19}$$

where $\varphi_e=\frac{\sigma_e}{\sigma_1}$.

In the original Considère criterion, (dt/t) is replaced by $d\varepsilon_3$. Eq. (19) can thus be reduced as:

$$\varphi_e\frac{-ba\exp(b\varepsilon_{eq-i})}{1-a\exp(b\varepsilon_{eq-i})}=(\beta_1+\alpha\beta_2)(-\frac{\varphi_2}{\varphi}-\frac{\varphi_3}{\varphi}) \tag{20}$$

where the limit strain $\varepsilon_{eq\text{-}i}$ at the diffuse instability pointcan be obtained by solving Eq. (20).

In microforming of metal foil, free surface roughening plays an important role in the formation of necking. The Considère criterion is thus modified considering the physical modeling of free surface roughening. Here, (dt/t) is not equal to $d\varepsilon_3$. By substituting Eq. (12) into Eq. (19), (what is the logic link between these two statements???) the critical equivalent strain $\varepsilon_{eq\text{-}i}$ at the diffuse instability point is derived as:

$$\varphi_e\frac{-ba\exp(b\varepsilon_{eq-i})}{1-a\exp(b\varepsilon_{eq-i})}=(\beta_1+\alpha\beta_2)(-\frac{\varphi_2}{\varphi}-G) \tag{21}$$

where

$$G=\frac{(-\frac{\varphi_1}{\varphi}-\frac{\varphi_2}{\varphi})\exp(-\frac{\varphi_1}{\varphi}\varepsilon_{eq-i}-\frac{\varphi_2}{\varphi}\varepsilon_{eq-i})-\frac{2}{3}c\frac{d_0}{t_0}}{\exp(-\frac{\varphi_1}{\varphi}\varepsilon_{eq-i}-\frac{\varphi_2}{\varphi}\varepsilon_{eq-i})-\frac{2}{3}(c\frac{d_0}{t_0}\varepsilon_{eq-i}+\frac{R_0}{t_0})}.$$

Eq. (21) can be solved by using the iteration algorithm. When R_0 equals to 0 and t/d_0 approaches infinity, Eq. (21) is converged to the original Considère criterion, i.e., Eq. (20). (this is a very good statement! When you need to revise or modify an existing criterion, when it can be converged to the original one is a critical criterion)

3.3 M-K and PMC models

(1) M-K model

The concept of M-K model is schematically illustrated in **Fig. 8**. According to the original M-K model, the incipient groove in the original material will grow continuously with deformation. The initial value of the geometrical defect is characterized by $f_0 = t_0^B/t_0^A$ and t_0^A and t_0^B are the initial thicknesses of regions *A* and *B*, respectively. Generally, the value of the incipient groove is considered as an adjustable parameter to optimize the predicted forming limit curves. As the plastic deformation proceeds, the localized necking eventually occurs at region *B* when the failure criterion is satisfied.

Based on the Yld2000-2d yield criterion, force equilibrium and geometrical compatibility, the strain increment $d\varepsilon_{eq}^B$ in region *B* can be calculated by assuming a small increment of the equivalent strain $d\varepsilon_{eq}^A$ in region *A*. When the failure criterion $d\varepsilon_{eq}^B/\, d\varepsilon_{eq}^A \geq 7$ is satisfied, the major and minor principal strains accumulated in region *A* are defined as the limit strains. The detailed procedure used to calculate the FLCs was described in Ref. (Cheng et al., 2017b). It is found that the incipient groove is perpendicular to the principal axis-*1* in this research. (In other researches, it is not perpendicular to the principal axis-1??? If yes, why??)

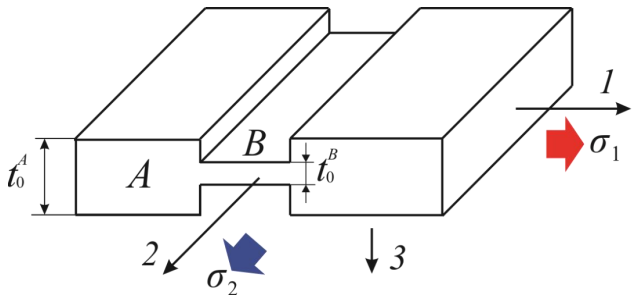

Fig. 8 The schematic diagram of the M-K model.

(2) PMC model

In the previous studies, many scholars have found that the surface roughness uniformly

evolves with plastic strain. The incipient groove in the original metal foil does not exhibit continuing growth until the diffuse instability condition is reached. It is inappropriate that the initial geometrical defect in the M-K model is assumed to grow continuously from the beginning of plastic deformation. Therefore, Parmar et al. (1977) proposed PMC model for determination of FLC. In the PMC model, the modified M-K model is applied after the diffuse instability point. The plastic deformation process is decomposed into two stages, including the homogeneous deformation up to load instability and the deformation localization until localized necking. In the first stage, the surface roughness is considered to follow the Considère criterion, as presented in Section 3.1. In the second stage, a single long groove is formed and developed into a strain localization. The modified M-K model is used to analyze the evolution of the long groove in the second stage. Therefore, the limit strain is the sum of the strain up to load instability and the strain from instability to localized necking.

However, one of the most challenging aspects in the PMC model is the definition of the initial imperfection f_i in the modified M-K model, which is set to be the thickness ratio at the diffuse instability point, i.e., $f_i = t_i^B / t_i^A$, as shown in **Fig. 9**. According to Bong et al. and Jain et al. (2012; 1996), t_i^A and t_i^B are the minimum thicknesses outside and inside the groove, respectively. Based on the equivalent strain $\varepsilon_{eq\text{-}i}$ at the diffuse instability point and the initial thickness t_0, t_i^A can be calculated by Eq. (5). As for t_i^B, it can be determined via the surface roughness.

$$\begin{cases} t_i^B = t_i^A - 2 * R_k \\ R_k = k * R_z \end{cases} \tag{22}$$

where R_z is the surface roughness and k is the surface roughness parameter, which is equal to 1 or 0.5 in the previous studies. In this research, k is defined as an adjustable parameter to achieve the best prediction. The stress states inside and outside the incipient groove are assumed to be the same at the diffuse instability point and the surface roughening will continue to grow after the instability point.

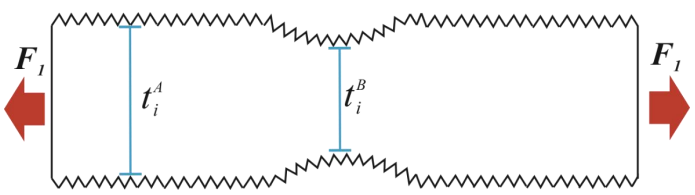

Fig. 9 Cross section of metal foil at the diffuse instability point.

According to the surface roughness effect, the current thickness of metal foil, t, can be determined by equating the overall volume of metal foil at diffuse instability point to the current volume and thus the following equation is established

$$\frac{t}{t_i} = \{1 + \frac{2}{3}\frac{c\frac{d_0}{t_0}\varepsilon_{eq\text{-}i} + \frac{R_0}{t_0}}{\frac{t_i}{t_0}}\}\exp(-d\varepsilon_1 - d\varepsilon_2) - \frac{2}{3}\frac{c\frac{d_0}{t_0}(d\varepsilon_{eq} + \varepsilon_{eq-i}) + \frac{R_0}{t_0}}{\frac{t_i}{t_0}} \quad (23)$$

where $d\varepsilon_1$, $d\varepsilon_2$ and $d\varepsilon_{eq}$ are the major principal, minor principal and equivalent strains of the current volume measured from the instability point. The suffix i refers to the diffuse instability point. Eq. (23) can be applied to both regions A and B.

According to the force equilibrium, Eq. (24) is obtained

$$t^A\sigma_1^A = t^B\sigma_1^B \quad (24)$$

Considering the same work-hardening in regions A and B, the following Eq. (25) is obtained by combining Eqs. (1), (23) with (24).

$$\frac{t^A}{t_i^A}\frac{[1 - a\exp(b(\varepsilon_{eq-i} + d\varepsilon_{eq}^A))]}{\varphi_e^A} = f_i\frac{t^B}{t_i^B}\frac{[1 - a\exp(b(\varepsilon_{eq-i} + d\varepsilon_{eq}^B))]}{\varphi_e^B} \quad (25)$$

where $d\varepsilon_{eq}^A$ and $d\varepsilon_{eq}^B$ are the equivalent strains of regions A and B measured from the instability point. f_i is the initial imperfection in the instability point and can be calculated by Eqs. (5) and (22). In addition, the geometrical compatibility is expressed as:

$$d\varepsilon_2^A = d\varepsilon_2^B \quad (26)$$

When the PMC model is used to predict the theoretical μ-FLC, the flow chart proposed and presented in **Fig. 10** will be employed. In the flowchart, α^A is the current stress state in region A.

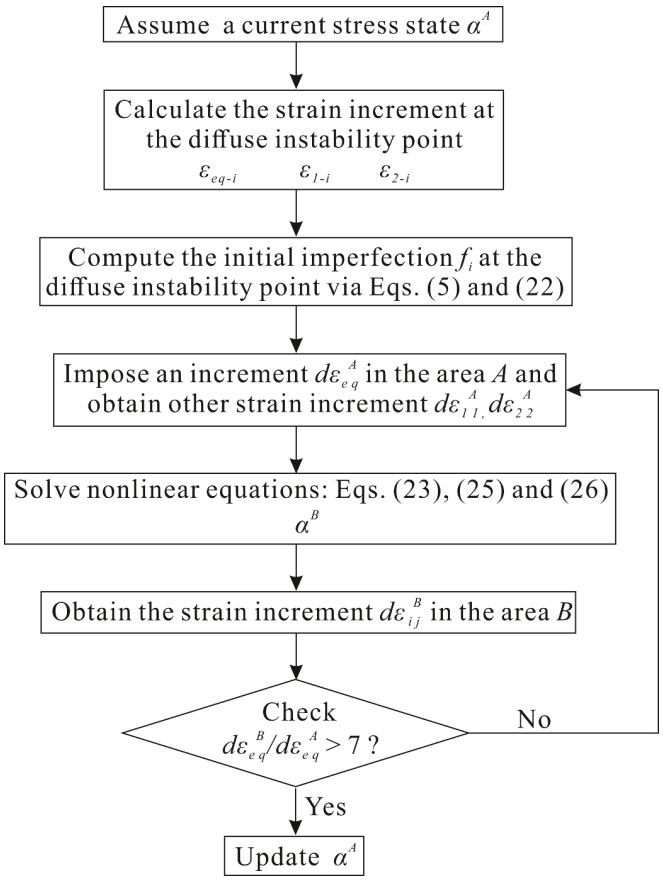

Fig. 10 Flow chart to calculate the theoretical μ-FLC based on the PMC model.

3. Results and discussion

4.1 Microscale failure behavior of metal foil

To accurately determine the forming limit of metal foils, the failure mechanism under different stress states was analyzed. The cross-sectional morphologies of the deformed specimens Nos. 1 and 6 shown in **Fig. 6** with the original thickness of 120 μm are illustrated in **Fig. 11**, which correspond to the uniaxial and biaxial tensile stress states. It is found that the fracture morphology varies with stress state and material condition. Under the equi-biaxial tensile stress state (Specimen No. 6), the thinning of material in the thickness direction is not obvious and the fracture morphology is similar to the knife-edge cross section. Under the uniaxial tensile stress state (Specimen No. 1), the material at the fracture point becomes more slenderized with the decrease of grain size and the corrugated fracture pattern across the thickness direction can also be observed. According to the definition of the load instability, the metal foil is uniformly deformed till the load acting on the foil cross section

reaches its maximum value. The cross section in the thickness direction is thus not significantly thinned before the diffuse instability point. After the loading instability, the deformation becomes intensively concentrated into the localized necking band, which causes the local thinning in the necking area. It is inferred from **Fig. 11** that the failure mechanism tends to transform from localized necking to diffuse instability with the change of stress state from uniaxial tension to equi-biaxial tension.

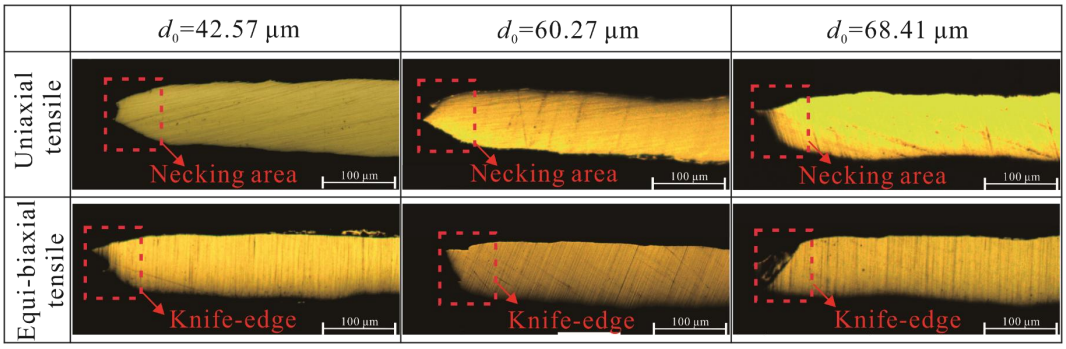

Fig. 11 Cross-sectional fracture morphology of the deformed samples at failure point.

In addition, scanning electron microscope (SEM) observations were conducted to study the size effect on failure mechanism. The SEM images of fracture surface with the thicknesses of 200 and 120 μm are shown in **Fig. 12**. As the thickness increases or the grain size decreases, the plentiful dimples and elongated microvoids were found on the fracture surface. On the contrary, it is observed that few microvoids and the obvious knife edge rupture appearred on the fracture surface under the coarse grain size or thinner foil thickness conditions. According to the previous studies (Fu and Chan, 2011; Klein et al., 2001; Meng et al., 2018), when the metal foil thickness is in the order of grain size, the deformation behavior tends to be the single crystal slip deformation and the non-uniform distribution of deformation accelerates the formation of cracks and leads to the premature fracture. Therefore, the microvoids on the shear dominant fracture surface are rarely found when the size effect is obvious. However, when the size effect is not remarkable, the large plastic deformation of material leads to the formation of microvoids in the grain boundaries, and the fracture surface characterized by the nucleation, growth and coalescence of microvoids demonstrates that the localized necking is the dominant failure mechanism.

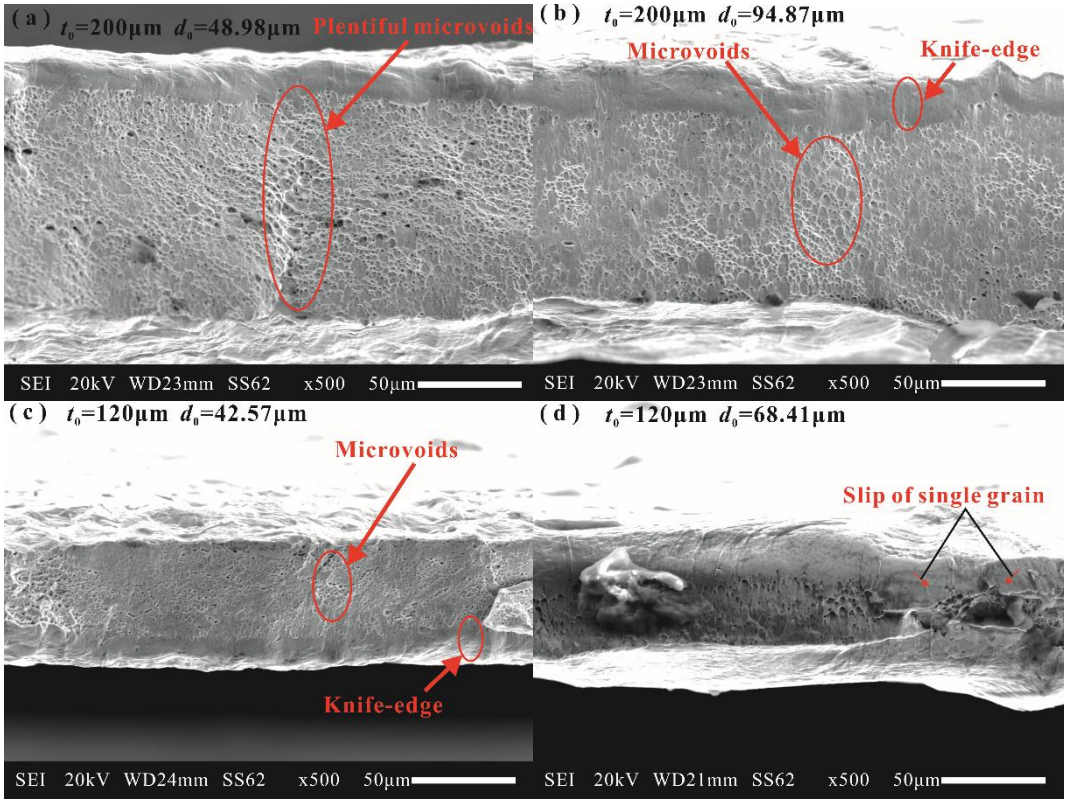

Fig. 12 SEM images of fracture surface with different material conditions (unit: μm) : (a) t_0 = 200, d_0 = 48.98 (b) t_0 = 200 , d_0 = 94.87; (c) t_0 = 120, d_0 = 42.57 and (d) t_0 = 120, d_0 = 68.41.

The evolution of strain paths under different stress states and material conditions was also used to reveal the failure mechanism of metal foils. **Fig. 13** shows the variations of the strain ratio ρ under uniaxial tensile (Specimen No. 1) and equi-biaxial tensile (Specimen No. 6) states, which is defined as $\varepsilon_2/\varepsilon_1$. Obviously, the strain ratio ρ of Specimens No. 1 deviates from the uniaxial stress state and is getting closer to the plane strain state with the increasing grain size and the decreasing foil thickness. According to the research from Cheng et al. (2017a), the realization of the plane strain state is taken as the failure criterion of localized necking. The phenomenon that the stress state shifts to the plane strain state indicates that the plastic deformation in the localization stage is gradually decreased with the increasing grain size or the decreasing foil thickness. Therefore, the intensified size effect promotes the transformation of failure mechanism from the localized necking to diffuse instability. Furthermore, the strain ratio ρ of No. 6 specimen also deviates from the equi-biaxial stress state and tends more obviously to be the plane strain state. It is concluded that the

phenomenon of localized necking is inconspicuous under biaxial tensile state and the ductile fracture of metal foils is caused by the diffuse instability.

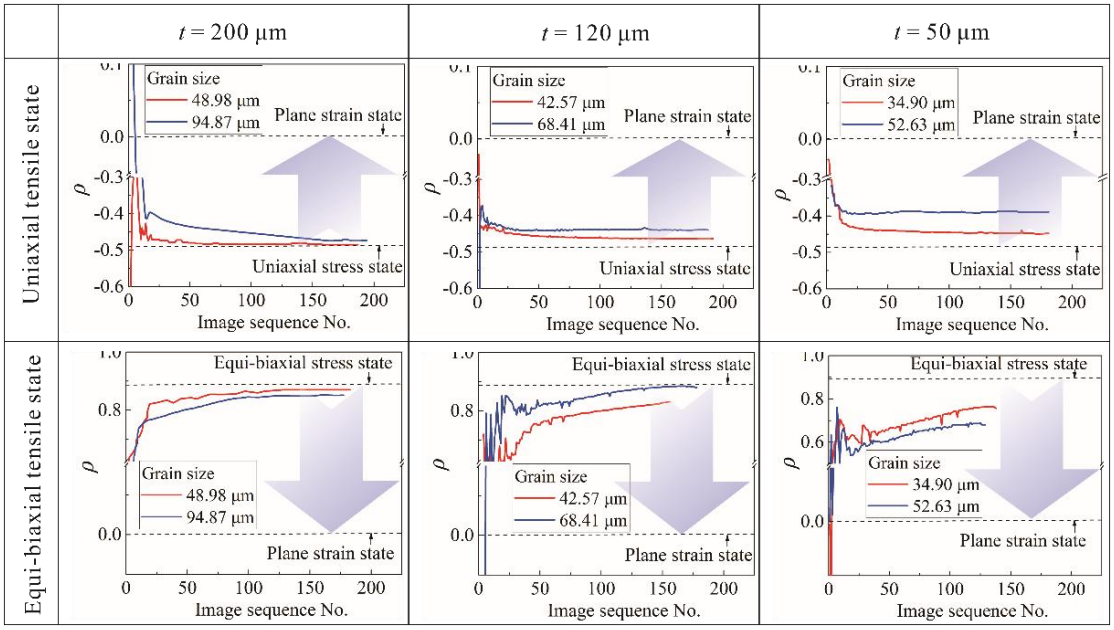

Fig. 13 Evolution of strain path under diverse stress states and material conditions.

4.2 Comparison of the experimentally and theoretically determined μ-FLC

According to Eq. (20), the μ-FLCs determined based on the original Considère criterion are shown in **Fig. 14**. The experimental results are also presented in **Fig. 14**. It is shown that the experimentally detemrined μ-FLC shifts down with the increasing grain size and the decreasing foil thickness, which can be explained by the surface layer model. According to surface layer theory, the internal layer becomes thinner with the decrease of t/d and promotes the coalescence of voids and the extension of micro crack in the thickness direction (Fang et al., 2015; Xu et al., 2015b). Although the right-hand-side μ-FLCs determined based on the original Considère criterion are obviously higher than the experimental results, the variation trend of the forming limit with stress state is similar to the experimental one, which is declined when the stress state changes from plane strain to equi-biaxial tensile state. However, the shape and size of the left-hand-side μ-FLCs cannot be predicted by the original Considère criterion. Moreover, it is also found the predicted μ-FLC is significantly affected by the hardening parameter b in Eq. (1). The smaller parameter b, the lower the theoretically determined μ-FLCs.

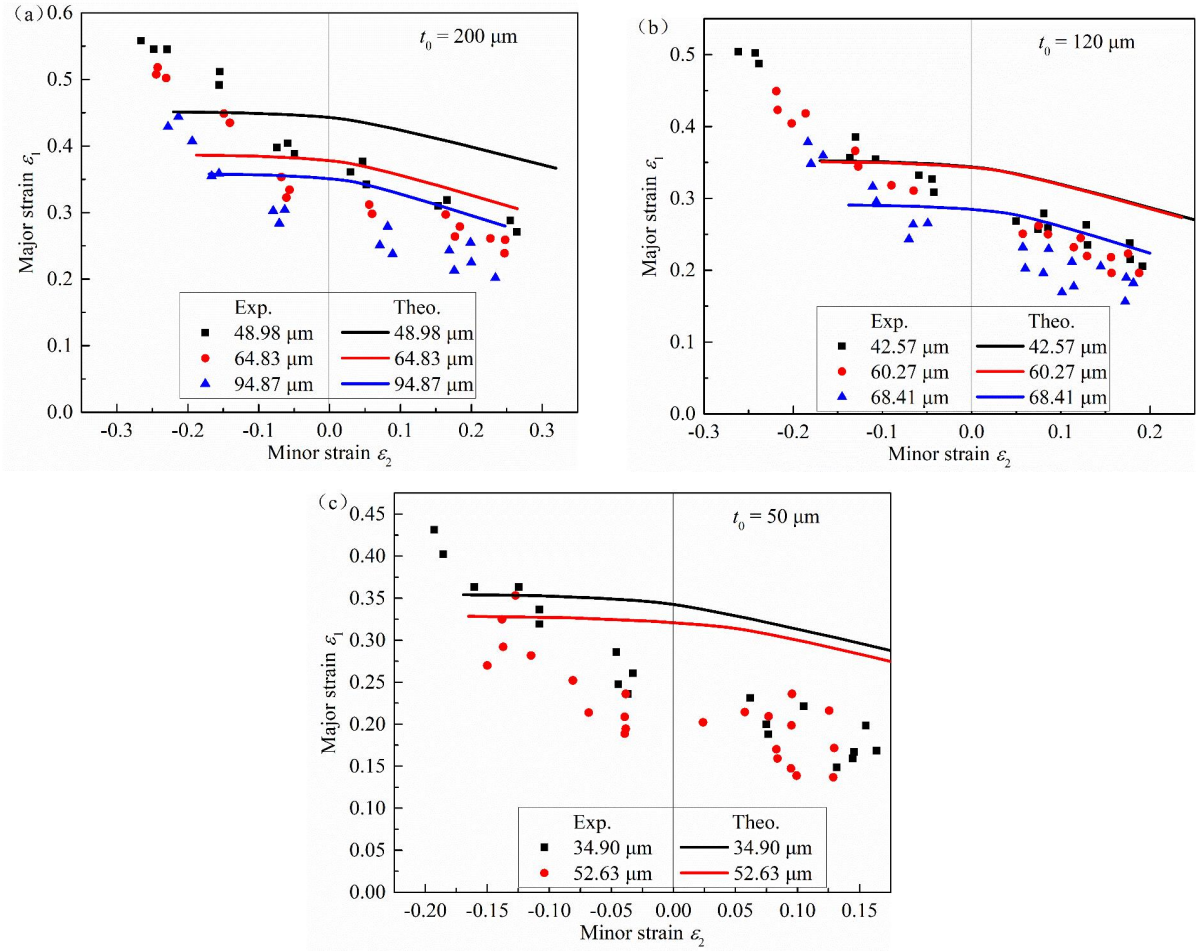

Fig. 14 Comparison of the μ-FLCs determined based on the original Considère criterion with the experimental ones: (a) 200 μm; (b) 120 μm and (c) 50 μm.

To expand the original Considère model to microscale, the theoretical μ-FLC was determined based on the modified criterion, i.e., Eq. (21). The theoretically determined μ-FLCs were then compared with the experimental results shown in **Fig. 15** (logic problem of this statement!!! To expand the original Considère model to microscale, you get the modified the modified criterion?). It is observed that the shape and size of the right-hand-side μ-FLC is accurately predicted by the modified Considère criterion. However, the μ-FLC at the negative minor strain region is underestimated by using the criterion. Combined with the original Considère criterion, it is concluded that the failure behavior under the biaxial stress state can be described by the modified Considère criterion considering free surface roughening. Whereas, the diffuse instability model is not suitable for prediction of the left-hand-side μ-FLC and the plastic deformation under the uniaxial stress state may proceed after the diffuse instability point. As analyzed in Section 4.1, the diffuse instability is the prominent failure mechanism under the biaxial stress state.

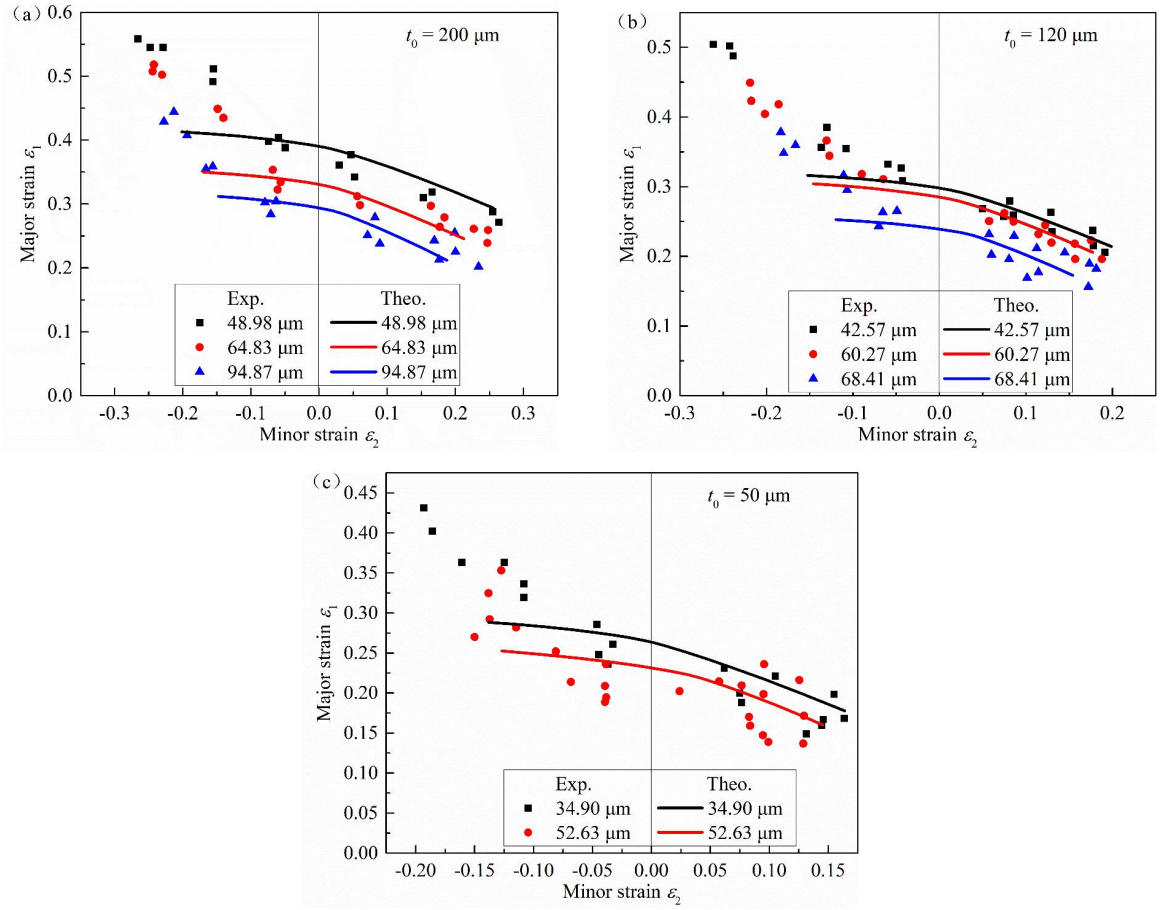

Fig. 15 Comparison of the μ-FLC determined based on the modified Considère criterion with the experimental ones: (a) 200 μm; (b) 120 μm and (c) 50 μm.

By using the original M-K model, the initial value of the geometrical defect f_0 is optimized by matching the predicted limit strain at the plane strain state with the experimental result for the metal foils with the thickness of 200 μm and the grain size of 48.98 μm. The theoretically determined μ-FLCs based on the M-K model are depicted in **Fig. 16**. It is revealed that the left-hand-side μ-FLC is slightly higher than the experimental forming limit strains, and the prediction deviation is aggravated with the increasing grain size and the decreasing foil thickness. Nevertheless, the right-hand-side μ-FLC is obviously overestimated based on the original M-K model. The theoretically determined right-hand-side μ-FLCs do not show the declining trend with the increase of grain size, especially for the foil with the t/d ratio less than one.

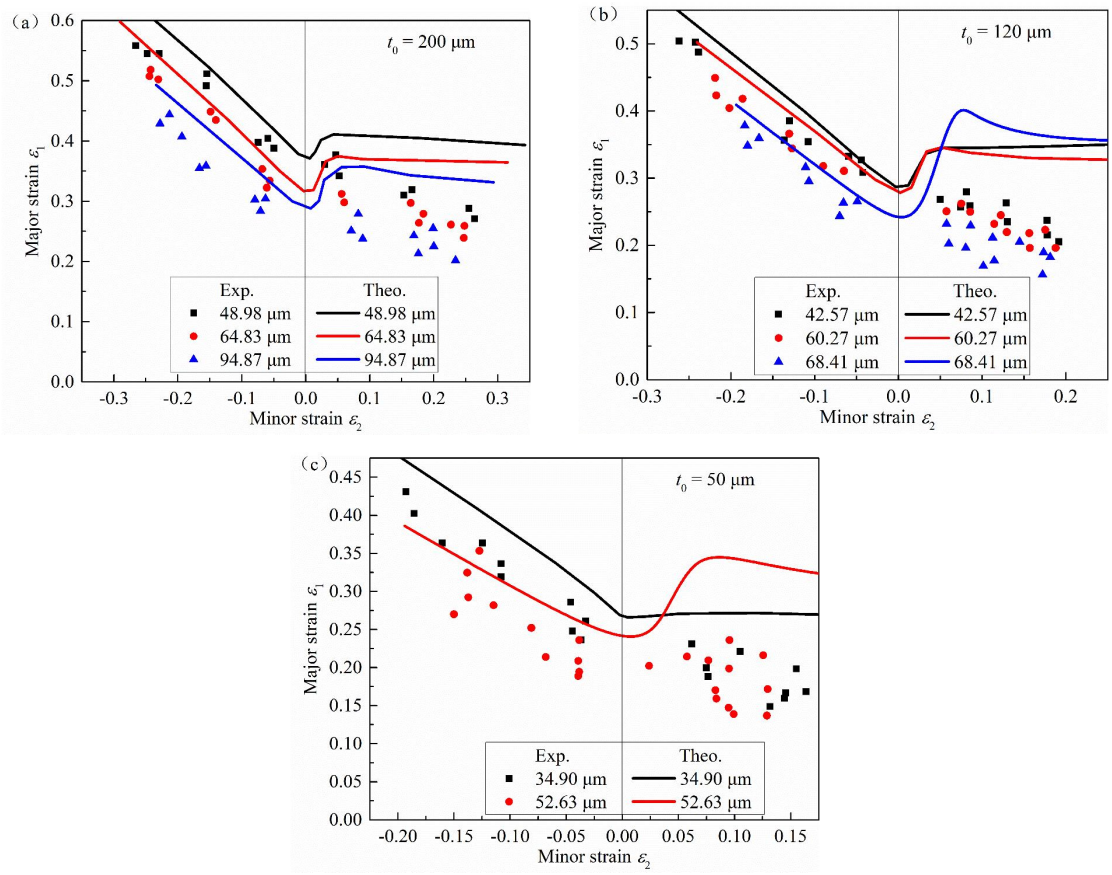

Fig. 16 Comparison of the μ-FLC determined by using the M-K model with the experimental ones: (a) 200 μm; (b) 120 μm and (c) 50 μm.

As for the PMC model, the initial imperfection f_i of the modified M-K in the second step is calculated according to Eqs. (5) and (22) (what is the relationship between the PMC model and the modified M-K? Is the latter used as the former???). The theoretically determined μ-FLCs based on the PMC model with the various values of the surface roughness parameter k are shown in **Fig. 17** for the metal foils with the thickness 200 μm and the grain size of 48.98 μm. In the vicinity of the plane strain state, the localized necking and diffuse instability are overlapped, which agree well with the experimental data. For the uniaxial or biaxial stress state, the plastic deformation in the localization stage is gradually decreased with the increase of the parameter k. It means that the growth of the surface roughness promotes the transformation of failure pattern from the localized necking to the diffuse instability. In addition, it is also observed from **Fig. 17(c)** that the right-hand-side μ-FLC determined based on the diffuse instability is consistent with the experimental results. The predicted left-hand-side μ-FLC also agrees well with the experimental result by the parameter k adjusted to 0.1. It is concluded that the PMC model with the adjustable surface roughness

parameter is suitable for determining the μ-FLCs at the negative minor strain region. Furthermore, it is further demonstrated that the localized necking is the dominant failure mechanism under the uniaxial stress state.

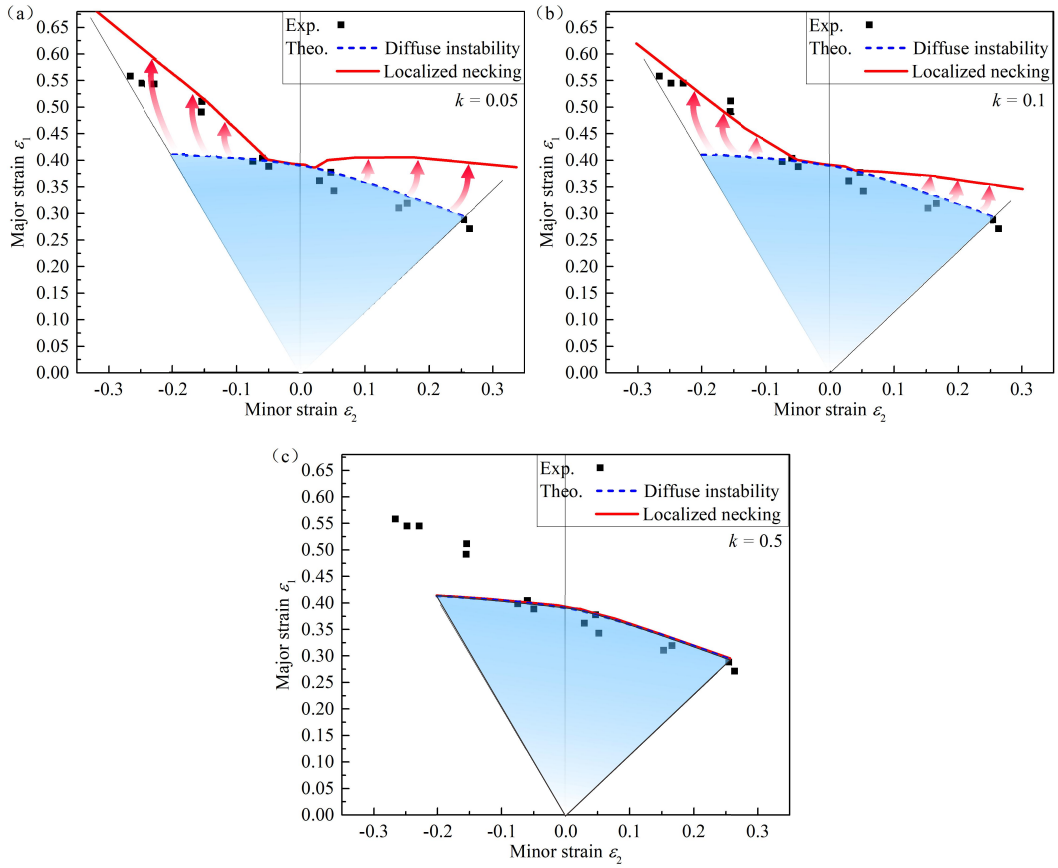

Fig. 17 Comparison of the μ-FLC determined based on the PMC with different values of the surface roughness parameter *k*: (a) 0.05; (b) 0.1 and (c) 0.5.

4.3 Modeling of diffuse instability considering stress state (??)

By comparing the predicted μ-FLC determined based on various failure models with the experimental results, it is revealed that the original Considère criterion and M-K model are not able to describe the intrinsic mechanism of the failure behavior of the metal foils well. The right-hand-side μ-FLC can be accurately predicted by the modified Considère criterion considering the size effect and the left-hand-side μ-FLC can be properly represented by the PMC model with an adjustable surface roughness parameter. It shows that the failure mechanism is related to the stress state. Under the biaxial stress state, the failure of metal foils is resulted from the diffuse instability. For the uniaxial stress state, the localized necking is the main cause. As for the boundary between diffuse instability and localized necking, it

needs to be carefully considered. As shown in **Fig. 17**, the boundary is not located at the plane strain state.

To determine the critical stress state for distinguishing different failure patterns in microscale deformation of metal foils, the applicability condition of the modified M-K model in the second step of PMC model was analyzed. If the failure criterion in the modified M-K model is satisfied at the diffuse instability point, the relationship between the increments of equivalent strains in regions *A* and *B* can be depicted as follows:

$$d\varepsilon_{eq-i}^{B} = 7 * d\varepsilon_{eq-i}^{A} \tag{27}$$

By combining Eqs. (25) and (27), the lower limit of the initial imperfection $f_{i\text{-}limit}$ in the modified M-K model under different stress states is deduced as:

$$f_{i-\lim it} = \varphi_e^B / \varphi_e^A * [1 - a\exp(b(\varepsilon_{eq-i} + d\varepsilon_{eq-i}^A))] / [1 - a\exp(b(\varepsilon_{eq-i} + 7d\varepsilon_{eq-i}^A))] \tag{28}$$

where φ_e^A and φ_e^B are the ratios of the equivalent stress to the major principal stress in region *A* and *B*, respectively, which can be determined by the assumed stress state α_A. Moreover, the initial imperfection at the diffuse instability point, $f_{i\text{-}instability}$, is also computed by using Eqs. (5) and (22). The $f_{i\text{-}limit}$ and $f_{i\text{-}instability}$ are demonstrated in **Fig. 18** for the metal foils with the thickness of 200 μm and the grain size of 48.98 μm. If $f_{i\text{-}instability}$ is lower than the $f_{i\text{-}limit}$, the localized necking does not happen and the modified M-K model in the second step of PMC model is invalid. As shown in **Fig. 18**, the diffuse instability is activated when the stress state is between 0.20 and 0.62, which corresponds to the overlapping section of μ-FLC presented in **Fig. 17**.

It is noted that the critical point on the left is set to be the critical stress state (α_C = 0.20), which is not at the plane strain state. When the stress state is below α_C, the $f_{i\text{-}instability}$ is above the $f_{i\text{-}limit}$ and the PMC model is valid to calculate the microscale forming limit. When the stress state is greater than α_C, the modified Considère model is selected. Consequently, the microscale forming limit of metal foils is predicted by the proposed sectionalized method, i.e., the left-hand-side and right-hand-side μ-FLCs are calculated by the modified PMC model and Considère criterion, respectively. Similarly, the μ-FLCs under various material conditions are obtained by using the above-mentioned method, as shown in **Fig. 19**. It is found that the

critical stress state is located at the left side of the plane strain state. The whole μ-FLC predicted by the sectionalized method agrees well with the experimental results, which demonstrates that the consideration of free surface roughening and failure mechanism transformation in calculation of the microscale forming limit is needed. In addition, the developed segmentation model is applicable to characterize the failure behavior of metal foils with one or less than one grain existing across the thickness.

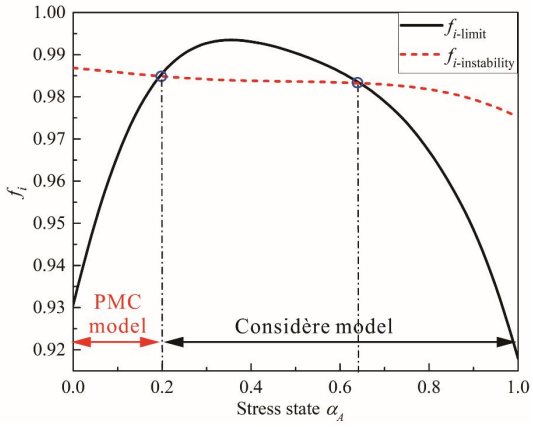

Fig. 18 The evolutionary trend of the $f_{i\text{-}limit}$ and $f_{i\text{-}instability}$ with stress state.

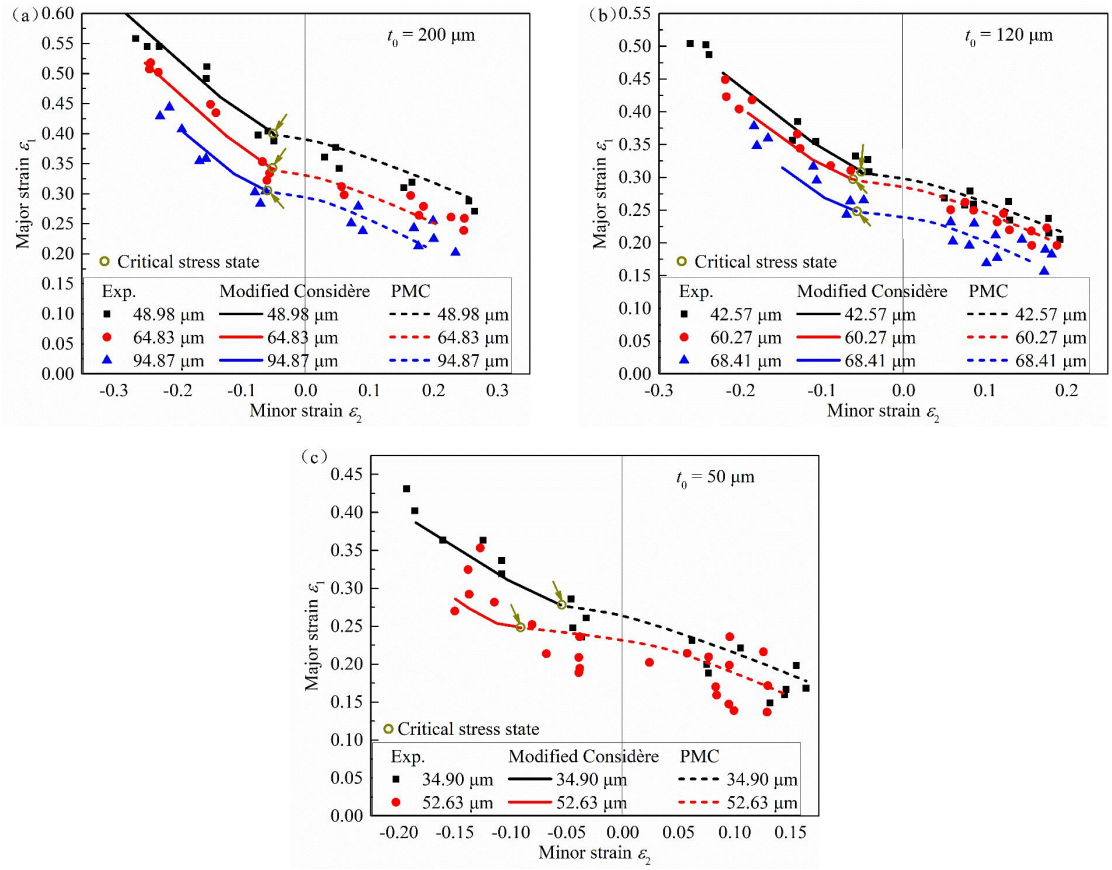

Fig. 19 The whole μ-FLC predicted by the modified Considère and PMC models.

According to **Fig. 19**, the failure pattern is distinguished by the critical stress state α_C. When the current stress state is lower than the critical stress state α_C, the localized necking is activated to calculate the left-hand-side μ-FLC. If the stress state is greater than the critical stress state α_C, the diffuse instability is valid and can be employed to construct the right-hand-side μ-FLC. Therefore, it is necessary to emphasize the size effect on the critical stress state α_C of metal foils. According to **Fig. 20**, the critical stress state α_C is gradually decreased and tends to be the uniaxial stress state ($\alpha = 0$) with the increasing grain size (d_0) or the decreasing foil thickness (t). It is suggested that the fracture pattern of metal foils presents a tendency of transition from localized necking to diffuse instability when the ratio of t/d is shifted down.

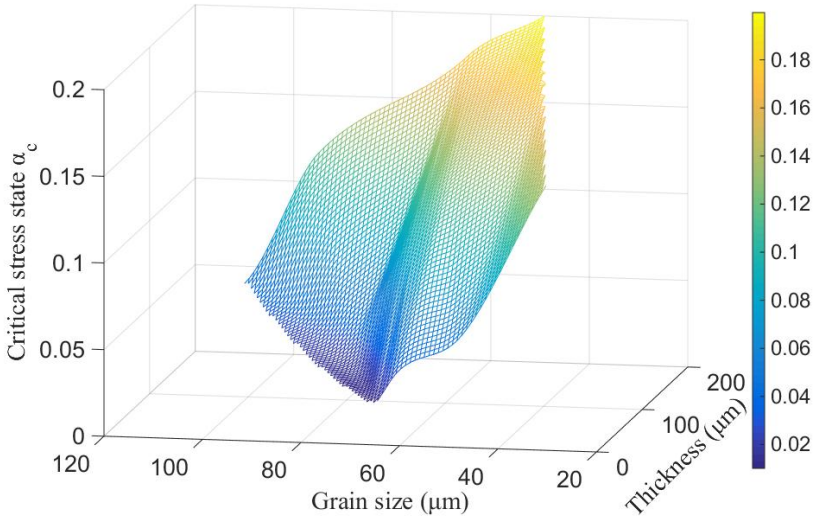

Fig. 20 Evolution of the critical stress state α_C under different material conditions.

5. Conclusion

In this research, the interactive effect of free surface roughening and stress state on the microformability and failure mechanism of metal foils in microscale deformation was sufficiently explored, and the sectionalized failure model was constructed to accurately determine the microscale forming limit of metal foils via considering the coupled effects of free surface roughening, failure mechanism transformation and scale dependent property. The main findings are summarized in the following:

(1) The free surface roughness of metal foils in microscale deformation is determined by the physical model with the pyramidal shape and proportional to the effective strain and grain

size, while the material constant is independent of grain size and foil thickness. (what the material constant???? You need to give the detail)

(2) The failure mechanism of metal foils tends to be transformed from localized necking to diffuse instability with the change of stress state from uniaxial tension to equi-biaxial tension. In addition, the increase of grain size or decrease of foil thickness promotes the transformation of fracture pattern from the localized necking to diffuse instability.

(3) The experimental μ-FLCs shifts down with the increasing grain size and the decreasing foil thickness and the much scattered limit strain is observed with only one or less grains existing over the thickness direction of metal foils. The original Considère criterion and M-K model are not suitable for predicting the microscale forming limit as they do not consider the significant effect of free surface roughening and failure mode transformation on the microformability of metal foils.

(4) A sectionalized failure criterion via introducing the critical stress state for distinguishing diverse failure mechanisms is developed to predict the microscale forming limit of metal foils. In detail, the modified Considère criterion coupling with free surface roughening is able to accurately determine the right-hand-side μ-FLC, while the modified PMC model by adjusting the surface roughness parameter and with the change of failure mechanism can predict the left-hand-side μ-FLC accurately. The proposed sectionalized failure model is able to characterize the fracture behavior of metal foils with one or less grains across the thickness direction. Furthermore, the critical stress state tends to be uniaxial stress state with the increasing grain size or the decreasing thickness of metal foils.

Acknowledgments

The authors would like to acknowledge the funding support to this research from the National Natural Science Foundation of China (Grant Nos.: 51635005, 51605018, 51575465 and 51504227), Beijing Natural Science Foundation (No. 3172022) and Graduate School of Beihang University.

References

Abe, T., 2014. Surface roughening and formability in sheet metal forming of polycrystalline metal based on r-value of grains. International Journal of Mechanical Sciences 86, 2-6.

Al-Qureshi, H.A., Klein, A.N., Fredel, M.C., 2005. Grain size and surface roughness effect on the instability strains in sheet metal stretching. Journal of Materials Processing

Technology 170, 204-210.

Barlat, F., Brem, J.C., Yoon, J.W., Chung, K., Dick, R.E., Lege, D.J., Pourboghrat, F., Choi, S.H., Chu, E., 2003. Plane stress yield function for aluminum alloy sheets—part 1: theory. International Journal of Plasticity 19, 1297-1319.

Bong, H.J., Barlat, F., Lee, M.G., Ahn, D.C., 2012. The forming limit diagram of ferritic stainless steel sheets: Experiments and modeling. International Journal of Mechanical Sciences 64, 1-10.

Chen, C.H., Lee, R.S., Gau, J.T., 2010. Size effect and forming-limit strain prediction for microscale sheet metal forming of stainless steel 304. Journal of Strain Analysis for Engineering Design 45, 283-299.

Cheng, C., Meng, B., Han, J.Q., Wan, M., Wu, X.D., Zhao, R., 2017a. A modified Lou-Huh model for characterization of ductile fracture of DP590 sheet. Materials & Design 118, 89-98.

Cheng, C., Wan, M., Wu, X.D., Cai, Z.Y., Zhao, R., Meng, B., 2017b. Effect of yield criteria on the formability prediction of dual-phase steel sheets. International Journal of Mechanical Sciences 133, 28-41.

Fang, Z., Jiang, Z., Wang, X., Zhou, C., Wei, D., Liu, X., 2015. Grain size effect of thickness/average grain size on mechanical behaviour, fracture mechanism and constitutive model for phosphor bronze foil. The International Journal of Advanced Manufacturing Technology 79, 1905-1914.

Fu, M.W., Chan, W.L., 2011. Geometry and grain size effects on the fracture behavior of sheet metal in micro-scale plastic deformation. Materials & Design 32, 4738-4746.

Fukui, Y., Nakanishi, K., 2008. Forming limit of sheet metal considering surface roughness. Transactions of the Japan Society of Mechanical Engineers 52, 833-840.

Furushima, T., Masuda, T., Manabe, K., Alexandrov, S., 2011. Inhomogeneous 3D Finite Element Model for Prediction of Free Surface Roughening. Advanced Materials Research 418-420, 1040-1043.

Furushima, T., Tsunezaki, H., Hirose, Y., 2018. Fracture and surface roughening behaviors in micro metal forming. Procedia Manufacturing 15, 1481-1486.

Furushima, T., Tsunezaki, H., Manabe, K.-i., Alexsandrov, S., 2014. Ductile fracture and free surface roughening behaviors of pure copper foils for micro/meso-scale forming. International Journal of Machine Tools and Manufacture 76, 34-48.

Gau, J.-T., Chen, P.-H., Gu, H., Lee, R.-S., 2013. The coupling influence of size effects and strain rates on the formability of austenitic stainless steel 304 foil. Journal of Materials Processing Technology 213, 376-382.

Guangnan, C., Huan, S., Shiguang, H., Baudelet, B., 1990. Roughening of the free surfaces of metallic sheets during stretch forming. Materials Science and Engineering: A 128, 33-38.

Jain, M., Lloyd, D.J., MacEwen, S.R., 1996. Hardening laws, surface roughness and biaxial tensile limit strains of sheet aluminium alloys. International Journal of Mechanical Sciences 38, 219-232.

Jain, V.K., Sidpara, A., Balasubramaniam, R., Lodha, G.S., Dhamgaye, V.P., Shukla, R., 2014. Micromanufacturing: A review—Part I. Proceedings of the Institution of Mechanical Engineers Part B Journal of Engineering Manufacture 228, 1-22.

Klein, M., Hadrboletz, A., Weiss, B., Khatibi, G., 2001. The ‘size effect’ on the stress–strain, fatigue and fracture properties of thin metallic foils. Materials Science and Engineering: A 319-321, 924-928.

Lai, X., Peng, L., Hu, P., Lan, S., Ni, J., 2008. Material behavior modelling in micro/meso-scale forming process with considering size/scale effects. Computational Materials Science 43, 1003-1009.

Mahmudi, R., Mehdizadeh, M., 1998. Surface roughening during uniaxial and equi-biaxial stretching of 70-30 brass sheets. Journal of Materials Processing Technology 80-81, 707-712.

Manabe, K., Shimizu, T., Koyama, H., Yang, M., Ito, K., 2008. Validation of FE simulation based on surface roughness model in micro-deep drawing. Journal of Materials Processing Technology 204, 89-93.

Meng, B., Fu, M.W., 2015. Size effect on deformation behavior and ductile fracture in microforming of pure copper sheets considering free surface roughening. Materials & Design 83, 400-412.

Meng, B., Fu, M.W., Fu, C.M., Chen, K.S., 2015. Ductile fracture and deformation behavior in progressive microforming. Materials & Design 83, 14-25.

Meng, B., Zhang, Y.Y., Cheng, C., Han, J.Q., Wan, M., 2018. Effect of plastic anisotropy on microscale ductile fracture and microformability of stainless steel foil. International Journal of Mechanical Sciences 148, 620-635.

Nurcheshmeh, M., Green, D.E., 2016. Prediction of forming limit curves for nonlinear loading paths using quadratic and non-quadratic yield criteria and variable imperfection factor. Materials & Design 91, 248-255.

Osakada, K., Oyane, M., 1971. On the Roughening Phenomenon of Free Surface in Deformation Process. Transactions of the Japan Society of Mechanical Engineers 36, 1017-1022.

Parmar, A., Mellor, P.B., Chakrabarty, J., 1977. A new model for the prediction of instability and limit strains in thin sheet metal. International Journal of Mechanical Sciences 19, 389-398.

Peng, L., Xu, Z., Gao, Z., Fu, M.W., 2017a. A constitutive model for metal plastic deformation at micro/meso scale with consideration of grain orientation and its evolution. International Journal of Mechanical Sciences.

Peng, L.F., Xu, Z.T., Fu, M.W., Lai, X.M., 2017b. Forming limit of sheet metals in meso-scale plastic forming by using different failure criteria. International Journal of Mechanical Sciences 120, 190-203.

Pham, C.H., Thuillier, S., Manach, P.-Y., 2015. Mechanical Properties Involved in the Micro-forming of Ultra-thin Stainless Steel Sheets. Metallurgical and Materials Transactions A 46, 3502-3515.

Ran, J.Q., Fu, M.W., 2014. A hybrid model for analysis of ductile fracture in micro-scaled plastic deformation of multiphase alloys. International Journal of Plasticity 61, 1-16.

Razali, A.R., Qin, Y., 2013. A Review on Micro-manufacturing, Micro-forming and their Key Issues. Procedia Engineering 53, 665-672.

Sène, N.A., Balland, P., Arrieux, R., Bouabdallah, K., 2013. An Experimental Study of the Microformability of Very Thin Materials. Experimental Mechanics 53, 155-162.

Stachowicz, F., 2016. On the connection between microstructure and surface roughness of brass sheets and their formability. Acta Mechanica 227, 253-262.

Tadros, A.K., Mellor, P.B., 1975. Some comments on the limit strains in sheet metal stretching. International Journal of Mechanical Sciences 17, 203-210.

Vollertsen, F., Schulze Niehoff, H., Hu, Z., 2006. State of the art in micro forming. International Journal of Machine Tools and Manufacture 46, 1172-1179.

Xu, J., Zhu, X., Shan, D., Guo, B., Langdon, T.G., 2015a. Effect of grain size and specimen dimensions on micro-forming of high purity aluminum. Materials Science and Engineering: A 646, 207-217.

Xu, Z.T., Peng, L.F., Fu, M.W., Lai, X.M., 2015b. Size effect affected formability of sheet metals in micro/meso scale plastic deformation: Experiment and modeling. International Journal of Plasticity 68, 34-54.

Xu, Z.T., Peng, L.F., Lai, X.M., Fu, M.W., 2014. Geometry and grain size effects on the forming limit of sheet metals in micro-scaled plastic deformation. Materials Science and Engineering: A 611, 345-353.

Yamaguchi, K., Takakura, N., Imatani, S., 1995. Increase in forming limit of sheet metals by removal of surface roughening with plastic strain (Balanced biaxial stretching of aluminium sheets and foils). Journal of Materials Processing Technology 48, 27-34.

Zhang, L., Wang, J., 2012. Modeling the localized necking in anisotropic sheet metals. International Journal of Plasticity 39, 103-118.